Int. J. Electrochem. Sci., 8 **(2013)** 2778 - 2790

International Journal of
ELECTROCHEMICAL
SCIENCE
www.electrochemsci.org

Assessment of the Corrosion Resistance of Fermanal Steel Coated With TiC(N)/TiNb(CN) Heterostructures for Use As a Biomaterial

W. Aperador[1,*], *J.C. Caicedo*[2], *R. Vera*[3]

[1]Departament of Engineering, Universidad Militar Nueva Granada, Carrera 11 No. 101-80, Fax:+57(1) 6343200, Bogotá, Colombia.
[2] Tribology Group, Polymers, Powder and Solid Residue Transformation Metallurgy - TPMR, Universidad del Valle, Cali – Colombia.
[3] Corrosion Laboratory, Chemistry Institute, Pontificia Universidad Católica de Valparaíso, Avda. Universidad, 330, Placilla, Valparaíso, Chile.
[*]E-mail: g.ing.materiales@gmail.com

Received: 14 December 2012 / *Accepted:* 8 January 2013 / *Published:* 1 February 2013

This study aims to assess corrosion resistance on multilayer coatings of [TiCN/TiNbCN]n in a physiological medium with 1, 50 and 150 bilayer periods deposited on silicon (100) and Fermanal steel (FeMnAl) substrates using R.F. reactive magnetron sputtering with a radio frequency source (13.56 MHz) and two TiC and Nb targets. The multilayers were characterized using X-ray diffraction (XRD) and scanning electron microscopy (SEM). The electrochemical behavior simulated by the corporal environment was assessed using electrochemical impedance spectroscopy and *Hanks* solution as the electrolyte. The morphology of the attack mechanism on the coated and uncoated steel samples was characterized using SEM. The corrosion products were assessed using XRD. A notable increase was observed in corrosion resistance with the deposits of multilayer coatings on the FeMnAl alloy substrates, suggesting the spatial period effect (Λ) in the decreased degradation seen on the coatings. This result corroborates the benefits of varying the bilayer period.

Keywords: Biomaterials, Fermanal, TiCN/TiNbCN, Hanks solution.

1. INTRODUCTION

The field of biomaterials has seen significant advances in recent years. One of the main reasons for this is the considerable increase in human life expectancy, which is reflected by the accelerated growth in the use of prostheses, implants and medical systems and devices which work in contact with body tissue [1,2].

Metals are used a biomaterials due to their excellent thermal and electrical conductivity and their mechanical properties [1]. They may be used in their pure form or as alloys in different phases, as a result of thermal treatment processes, or as coatings [3]. The metals in their pure form lack the properties required by different types of implants currently used in traumatology and orthopedics. This is the case with pure titanium, the use of which is constrained by its limited mechanical properties [4]. As a result it is necessary to add one or two metals to the base element in order to modify its crystalline structure and in turn its physical and chemical properties. An example of this is the Ti-6Al-4V alloy, although in recent years controversy has arisen over is biocompatibility [5].

There is currently a push towards the development of new alloys that do not contain vanadium but rather a low percentage of aluminum. The aim it to obtain alloys with improved biocompatibility in order to ensure a high level of performance in the human body over long periods when used in the manufacture of surgical implants [6]. AISI 316LVM stainless steel is used for medical applications because its manufacture process of vacuum melting achieves the high levels of purity necessary for surgical prostheses. It provides excellent resistance to physiological tissues and fluids, to intergranular corrosion and to corrosion in general [7-8]. However, its use as a biomaterial has been called into question as it contains nickel; this is because some individuals present an allergic reaction to this metal [9].

Iron (Fe), Manganese (Mn) and Aluminum (Al)-based alloys, known as Fe-Mn-Al, have gained enormous interest in recent years, mainly from a technological perspective, due to their similarity to conventional stainless steels produced using the ternary alloy Fe-Ni-Cr. In these steel alloys, the chrome stabilizes the ferric phase, producing a very fine passivating chrome oxide surface layer that protects the steel from subsequent rusting [10-12]. The same role is played by the aluminum in different FeMnAl alloys by stabilizing the austenite phase. This phase has better mechanical properties than FeCr containing steels. Manganese performs the same function in other Fermanal alloys [13-14]. The advantages of Fe-Mn-Al-based steel, in comparison to conventional steels, are its lower cost, excellent mechanical properties and good oxidation resistance [15]. These characteristics make such steels apt for different applications, from biomedical uses to the manufacture of receptacles for handling substances at cryogenic temperatures [16].

Corrosion in surgical implants can be critical, affecting the biocompatibility of the implant and the structural integrity of the prosthesis. Corrosion and dissolution of surface layers are two mechanisms that can lead to the introduction of metal ions into the human body. Biological reaction with these elements can cause a diverse range of effects [9]. Prostheses, dental implants and surgical tools are applications of biomaterials that take advantage of coatings generated by physical vapor deposition (PVD). The main value for such applications is the biocompatibility together with improved surface hardness and corrosion resistance. TiCN films have been deposited using PVD on AISI 316L stainless steel substrates. This process has shown high levels of corrosion resistance [17], while, in addition, in vitro assays with these coatings do not display cytotoxicity or genotoxicity [18-19].

Therefore, the present article proposes the study of Fe-Mn-Al alloys coated with multilayers of [TiCN/TiNbCN]n with 1, 50 and 150 bilayer periods, while assessing and enhancing their properties through the use of heterostructures that give improved corrosion resistance and biocompatibility.

2. MATERIALS AND METHODS

2.1 Materials

The Fermanal (FeMnAl) alloy was prepared using high purity materials by melting in an induction oven in an Argon atmosphere. Ingots were forged at 1200 °C and were homogenized at the same temperature for a period of 12 hours. They were then subjected to a thermal aging treatment at 600 °C for 18 hours followed by cooling in air. Finally, they were cut into slices 3±0.2 mm thick. The hardness obtained for the alloy was 29.1$HRB_{0,1}$. The composition of the sample is shown in Table 1. The probes used in the assays were 14 mm in diameter and 2.5 mm thick.

Table 1. Chemical composition of Fermanal alloy (%).

Elements	Al	Mn	C	Cu	Cr	Si	Mo	Fe	P	S	Ni	V
Alloy	6.40	17.02	0.46	0.01	2.99	0.08	0.05	72.6	0.03	0.24	0.04	0.005

2.2 Coating Application

The [TiCN/TiNbCN]n multilayers were deposited on silicon substrates with crystallographic orientation (100) for the purposes of measuring their structure, morphology and chemical composition, and on Fermanal steel substrates for measurement of degradation properties. The coatings were obtained through a combination technique of sputtering, denominated r.f. reactive magnetron sputtering (PVD), together with a negative r.f. polarization voltage applied to the different substrates. Two targets were used: stoichiometric titanium carbide, TiC, and niobium, Nb, both 4 inches in diameter, ~5 mm thick and 99.99% pure. All substrate surfaces were cleaned of organic contaminants in an ultrasonic bath in the sequence of ethanol and acetone for 15 minutes each. Prior to deposition, the vacuum chamber was evacuated using a turbomolecular pump until a base pressure of 7.2 $x10^{-5}$ mbar is attained in order to reduce the effects of residual air. Inside the chamber the substrates were subjected to a bias voltage of -400 V (r.f.) with a potential of 60 W (r.f.) in argon plasma (Ar) for 15 minutes in order to remove other contaminating impurities from the surfaces. The cathodic pulverization apparatus includes a system for positioning the substrate relative to the target. This can be used to vary the bilayer number (n) from 1 to 50 to 150, thus modifying the bilayer period (Λ). The total thickness of the deposited [TiCN/TiNbCN]n multilayers was approximately 3 µm for all coatings. The individual thickness varied depending on the number of bilayers from n = 1 to n = 150 layers produced with a period from 15 nm to 1.5 µm, respectively.

2.3 Assessment techniques

A Gamry model PCI-4 potentiostat-galvanostat was used to assess corrosion resistance in steady-state conditions. Electrochemical impedance spectroscopy (EIS) was used. The electrochemical corrosion assays were carried out at 37±0.2°C using Hanks solution (Hanks balanced salt solution,

Sigma) as the electrolyte. The chemical composition of the solution is shown in Table 2. The assays were performed as a function of time, over periods of 0, 48 and 192 hours.

Table 2. Chemical composition of electrolyte (Hanks solution).

Compound	Concentration (g/l)
NaCl	8
D-Glucose	1
$MgSO_27H_2O$	0.7
Na_2HPO_4	0.48
KCl	0.4
$NaHCO_3$	0.35
$CaCl_2.H_2O$	0.18
$MgO_2.6H_2O$	0.08
KH_2PO_4	0.06

A cell comprising a platinum counter-electrode, an Ag/AgCl reference electrode and the FeMnAl alloys with and without the [TiCN/TiNbCN]n coating with a exposed area of 1 cm^2 was used in the tests. Nyquist plots were obtained using frequency scanning in the range of 0.001 Hz to 100 kHz with sinusoidal signal amplitude of 10 mV. The development of the growth of the TiCN/TiNbCN multilayers was observed using a Scanning Electron Microscope (SEM). For this purpose the samples were cut along their cross-section using a diamond point, thus allowing SEM analysis of the growth characteristics of all the layers. Both growth morphology and surface characteristics were determined using a Phenom FEI SEM installed with an optical light with a magnification range of 524-24,000X and a high sensitivity (multi-mode) detector for retro-dispersed electrons. SEM was used to study the microstructure of the samples at 0 hours of exposure and later at 192 hours. The corrosion products generated on the steel surface were identified using X-Ray Diffraction (XRD). The X-ray diffraction apparatus used was a PW3050/60 Goniometer (θ/θ) under an XPERT-PRO system using Cu-Kα 1.54 Å monochromatic radiation and operated at 40 kV and 40 mA at 25°C. The surface scan was carried out from 2θ = 20.01° to 2θ = 99.99° with a scanning step 2θ = 0.02° and a scan time of 1 second.

3. RESULTS AND DISCUSSION

3.1 XRD characterization of multilayers

Figure 1 shows the high angle X-ray diffraction patterns (HA-XRD) of the [TiCN/TiNbCN]n multilayers. They clearly display the evolution of the diffraction pattern intensity for the set of multilayers with the reduction in the bilayer period. This increase in intensity is likely due to the higher number of crystals oriented in the preferential direction (111). As can be seen in Figure 1, in general the increase in the number of bilayers and the decrease in the bilayer period leads to clear preferential orientation in the Bragg planes (111). This corresponds to an FCC structure and is also seen with the

individual Ti-C-N and Ti-Nb-C-N layers [20-22]. It can clearly be observed that the texture of the Ti-Nb-C-N layers is still constant under the preferential orientation (111) [23], which is seen with the multilayers with bilayer period Λ= 1.5 μm to the multilayers with Λ= 20 nm.

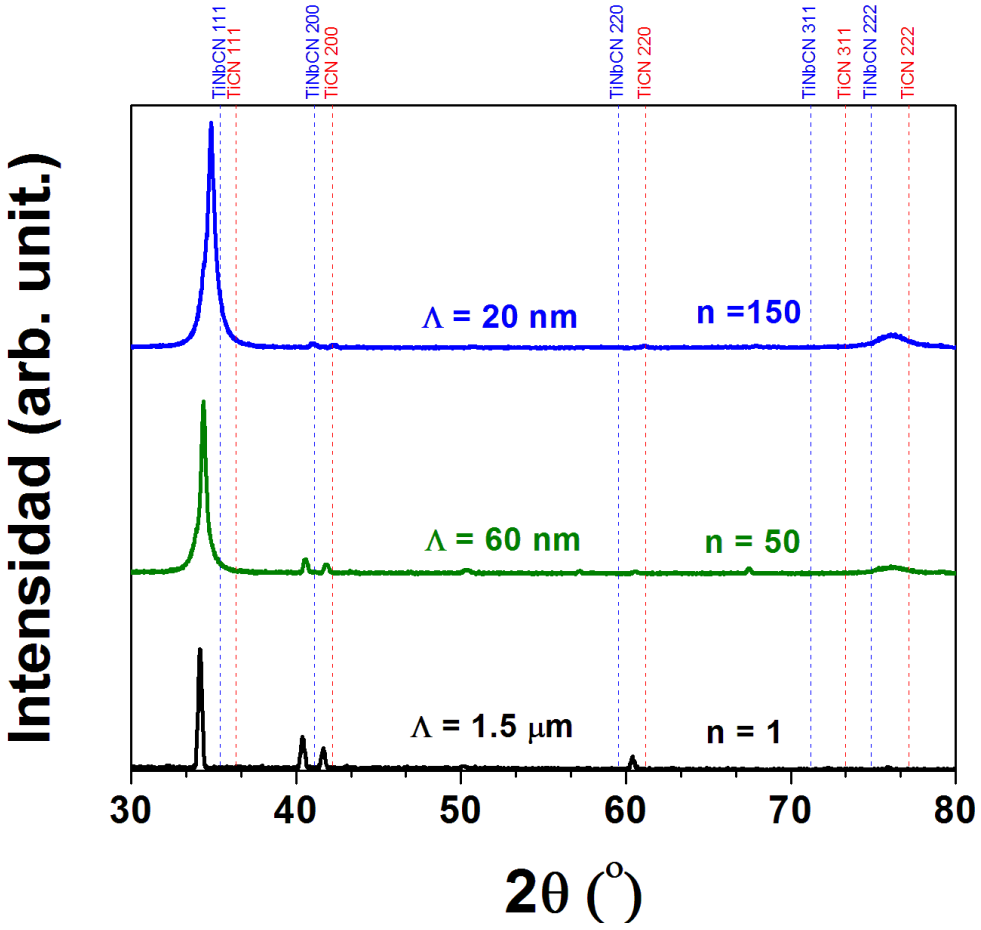

Figure 1. X-ray diffraction patterns for different TiCN/TiNbCN multilayers deposited on silicon (100).

3.2 Morphologic analysis via SEM

Figure 2a shows an image of the cross-section of a TiCN/TiNbCN (n=1) multilayer and figure 2b shows an image of the cross section of a TiCN/TiNbCN multilayer deposited with 50 bilayers (Λ= 60 nm). The darker contrast suggesting a change in chemical composition is a ternary layer of (Ti-C-N) in comparison to the quaternary layer of (Ti-Nb-C-N), which clearly demonstrates the structure and interfaces of the layers [24]. The TiCN/TiNbCN multilayers display a well-defined and uniform periodicity. Most of the multilayers were identified with SEM while the thickness values of the pre-designed bilayers were confirmed with a good degree of precision, as was the total thickness (3 μm). The only slight deviation seen in the SEM images was the relative thickness for multilayers with a very high number of bilayers or very small bilayer periods. The image in Figure 2a shows that the individual TiNbCN layers tend to be slightly thicker than the individual Ti-N-C layers. Despite the

analysis of the thickness of the multilayers with very thin individual layers around 7.5 nm, they are subject to spatial deviations which are difficult to evaluate due to the low resolution of the interfaces obtained by SEM.

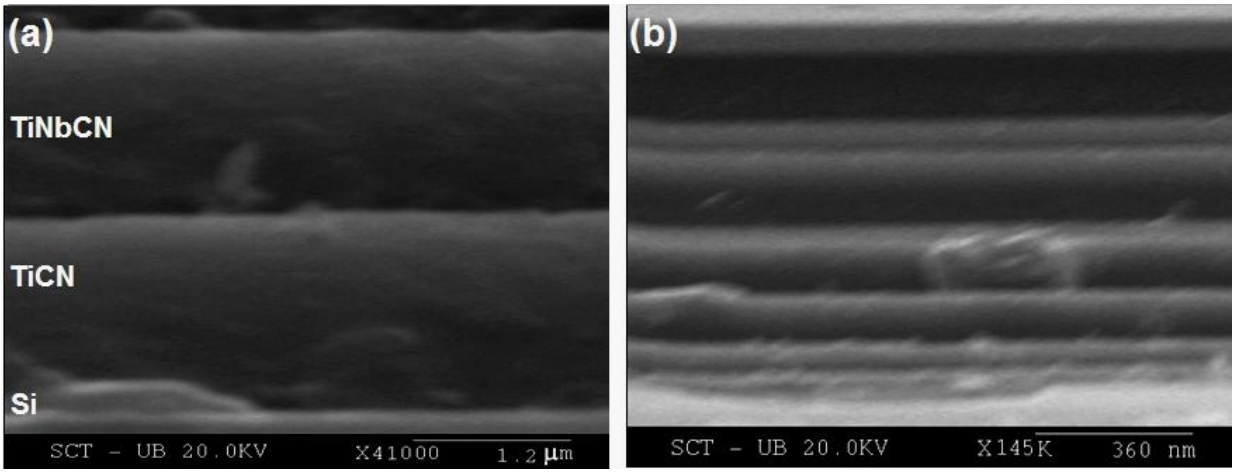

Figure 2. SEM micrographs of cross-sections of TiCN/TiNbCN multilayers: (a) n = 1, Λ = 1.5 µm; (b) n = 50, Λ = 60 nm.

3.2 Electrochemical assessment

Figures 3, 4 and 5 show the Nyquist plots of the response to the use of electrochemical impedance spectroscopy (EIS) to assess the action of the Hanks solution on the solution/coating interface. Exposure of the FeMnAl alloy with and without the [TiCN/TiNbCN]n coating in the biological solution was assessed in terms of time with evaluations at 0, 48 and 192 hours. The phenomena occurring over time on the interface suggest an increase in the protective effect after 0 hours of exposure. Figures 3, 4 and 5 also include the result of the simulation performed using the electric circuit shown in Figure 6. As can be seen, there is a good degree of concordance between the experimental and the simulated results. Table 3 presents the values for the parameters used in the simulation. These values were obtained using a complex nonlinear least squares (CNLS) program [25].

For the bilayers, a semi-defined semicircle is seen at high frequencies, while a better defined semicircle can be seen at low frequencies. These semicircles suggest interaction of two time constants. The semicircle found between100 kHz and 100 Hz is associated with the roughness of the coating surface, and also with organic compounds present in the electrolyte which have been absorbed onto the surface of the multilayers. At frequencies of 1Hz to 1 mHz, the behavior observed is attributable to corrosion processes that occur on the bilayer/substrate interface as seen in the changes in the Nyquist plots (Figures 3, 4 and 5), since the longer the immersion time, the higher the value of the electrochemical parameters. These changes indicate the protective capacity of the alloys under analysis.

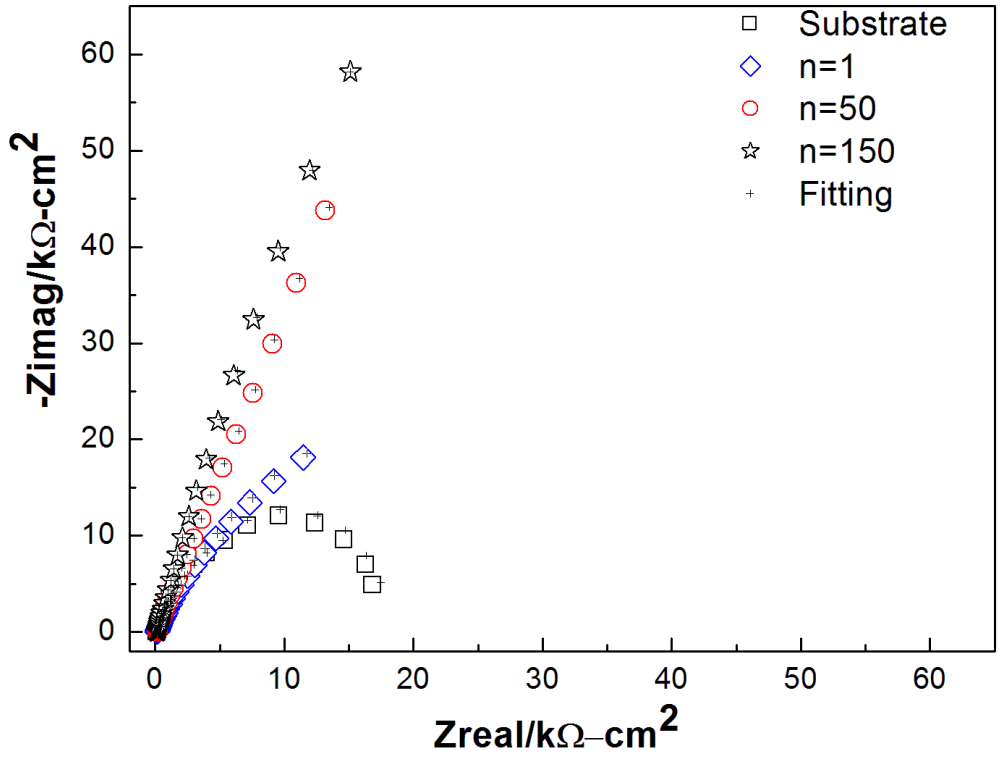

Figure 3. Nyquist plots of the [TiCN/TiNbCN]n multilayers evaluated at 0 hours.

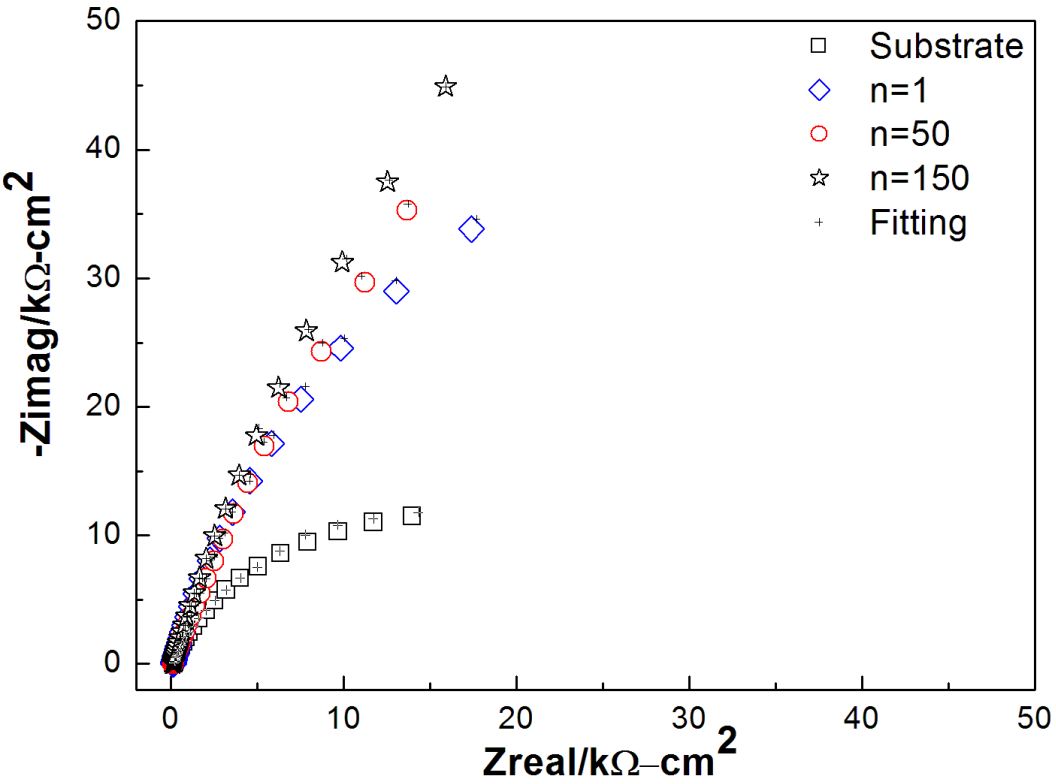

Figure 4. Nyquist plots of the [TiCN/TiNbCN]n multilayers evaluated at 48 hours.

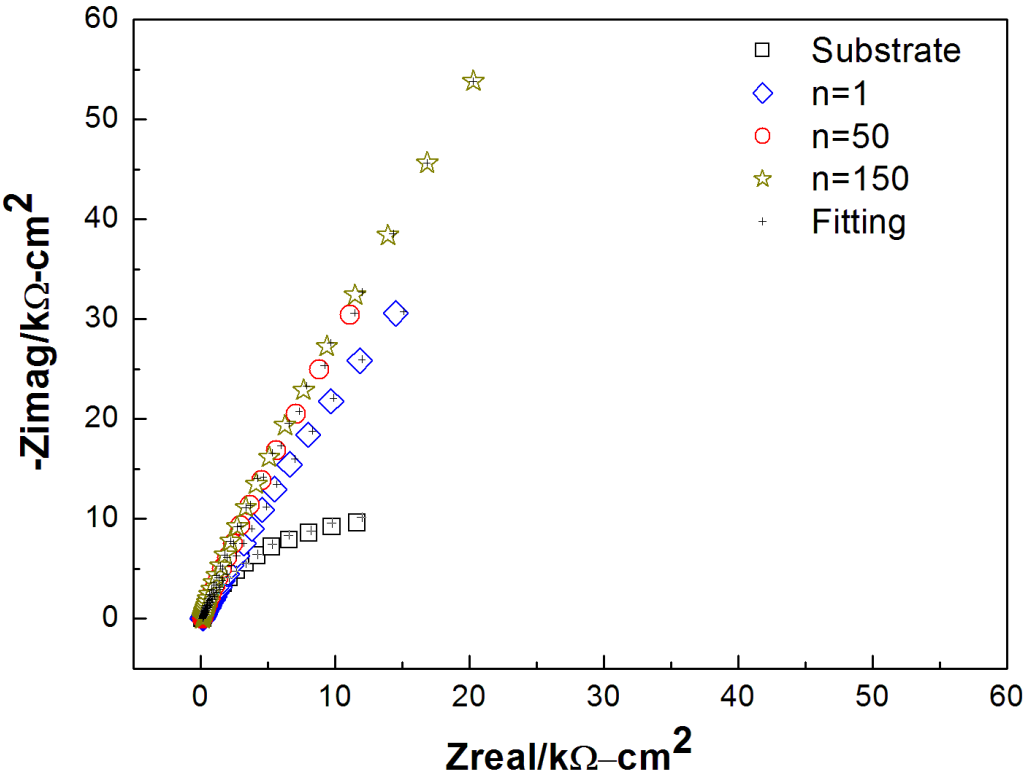

Figure 5. Nyquist plots of the [TiCN/TiNbCN]n multilayers evaluated at 192 hours.

The equivalent circuits in Figure 6 correspond to the Nyquist plots in Figures 3, 4 and 5. Two equivalent circuits were obtained in this study; a Randles circuit (Figure 6a) for the uncoated Fermanal steel, and another with 2 constant phase elements for the [TiCN/TiNbCN]n multilayers with bilayer periods of 1, 50 and 150 (Figure 6b). The diagram contains two capacitor elements labeled "double phase constant phase element" (CPE), which are independent of the faradic reactions that contribute a pseudo-capacitance (CPE2+CPE1) to the system's total impedance [25]. There is also an electrical resistance in the electrochemical cell associated with electrolyte resistance (Rs), which is also shown in the total impedance of the system. This resistance corresponds to the value contained in the Hanks solution. The CPE – R1 bond dominates at high frequencies, and may stem from the passive film, while the CPE2 – R2 bond controls the low frequencies and characterizes the properties of the bilayer/substrate interface [26].

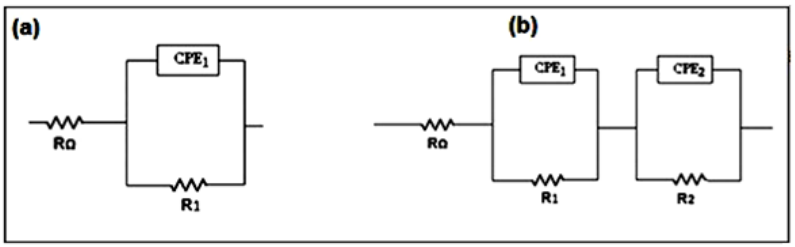

Figure 6. (a) Equivalent circuit used to fit substrate impedance data. (b) Equivalent circuit used to fit multilayer impedance data.

Table 3 shows the values of the parameters used in the simulation. These parameter values were obtained using a complex nonlinear least squares (CNLS) program [24]. The values for α (Table 3) are the exponential coefficient of the phase angle shift (π/2); the α-values for the coatings and the substrate for CPE at high frequencies are in the range of 0.79 to 0.92. This suggests that the roughness of the surface leads to charge distribution. For the CPE at low frequencies α = 0.56 at 0 hours, 0.68 at 48 hours and 0.72 at 192 hours for the 1 bilayer; for the 50 bilayers the values are 0.66 at 0 hours, 0.72 at 48 hours and 0.79 at 192 hours, suggesting that some species migration or diffusion is occurring. For 150 bilayers, the α-values are 0.87, 0.92 and 0.86 for 0, 48 and 192 hours, respectively. This implies the distribution of the density of charge carriers, i.e. a double layer with a complex structure. The total impedance data, i.e. the sum of all resistances, increases along with the increase in the number of bilayers (Table 3). It can also be seen that the total figures are much higher than those found for the substrate since the electrolyte is quite aggressive, and therefore causes a higher reaction rate on the uncoated steel [9].

Table 3. Electrochemical parameters obtained by EIS for the substrate and the coatings after 0, 48 and 192 hours.

	R_Ω (Ω cm^2)	CPE_1 (μF cm^{-2}) $s^{-(1-\alpha 1)}$	α_1	R_1 ($10^3\Omega$) cm^2	CPE_2 (μF cm^{-2}) $s^{-(1-\alpha 2)}$	α_2	R_2 ($10^3\Omega$ cm^2)
0 hours							
n=1	53.20 (0.5%)	1.59 (4.0%)	0.74 (0.2%)	2.23 (3.0%)	26.48 (2.0%)	0.56 (0.8%)	58.06 (4.0%)
n=50	63.30 (0.5%)	3.11 (0.5%)	0.69 (0.3%)	4.09 (3.0%)	35.32 (4.0%)	0.66 (0.9%)	114.32 (3.0%)
n=150	68.50 (0.7%)	4.37 (0.9%)	0.65 (0.6%)	5.21 (5.0%)	59.11 (3.0%)	0.87 (0.4%)	133.28 (3.0%)
Substrate	54.45 (0.6%)	63.38 (0.7%)	0.81 (0.6%)	19.34 (2.4%)			
48 hours							
n=1	68.30 (0.3%)	2.33 (3.0%)	0.78 (0.2%)	4.25 (5.0%)	32.95 (4.0%)	0.68 (0.6%)	98.75 (3.0%)
n=50	56.3 (0.6%)	4.82 (0.9%)	0.73 (0.5%)	5.34 (2%)	40.80 (3%)	0.72 (0.3%)	130.12 (4%)
n=150	58.80 (0.3%)	5.54 (1.2%)	0.74 (0.3%)	6.58 (4%)	62.24 (2%)	0.92 (0.5%)	190.31 (5%)
Substrate	64.50 (0.4%)	67.71 (1.6%)	0.83 (0.7%)	23.81 (3%)			
192 hours							
n=1	69.8 (0.2%)	3.48 (2%)	0.81 (0.4%)	5.05 (2%)	39.25 (5%)	0.72 (0.6%)	112.34 (4%)
n=50	63.7 (0.2%)	5.74 (0.4%)	0.79 (0.4%)	6.21 (5%)	46.21 (4%)	0.79 (0.3%)	141.86 (6%)
n=150	65.4 (0.6%)	6.21 (1.7%)	0.81 (0.4%)	8.12 (3%)	68.24 (3%)	0.80 (0.3%)	196.24 (3%)
Substrate	64.5 (0.4%)	86.24 (1.2%)	0.79 (0.4%)	27.32 (4%)			

3.3 Microstructural assessment of surfaces exposed to degradation

The surface characteristics of the Fermanal steel with (n=150 bilayers) and without the coating at 0 hours of exposure can be seen in the micrographs in Figures 7a and 7b. These images show the surfaces without any degradation due to contact with the Hanks solution. In Figure 7c it can be seen that part of the alloy has been deteriorated by the (simulated) hostile environment generated by the human body (37°C), which has altered the material by causing a change in its characteristics (depassivation), mainly as a result of corrosion and degradation. In the case of the multilayers, the surfaces eroded by the corrosion show a topographical change in the coatings, corroborating the findings of the EIS analysis, i.e. that the multilayer coating performs well. The deterioration seen in the multilayer surface, n = 150, shows the erosion that may occur under the conditions of simulated physiological fluids [28].

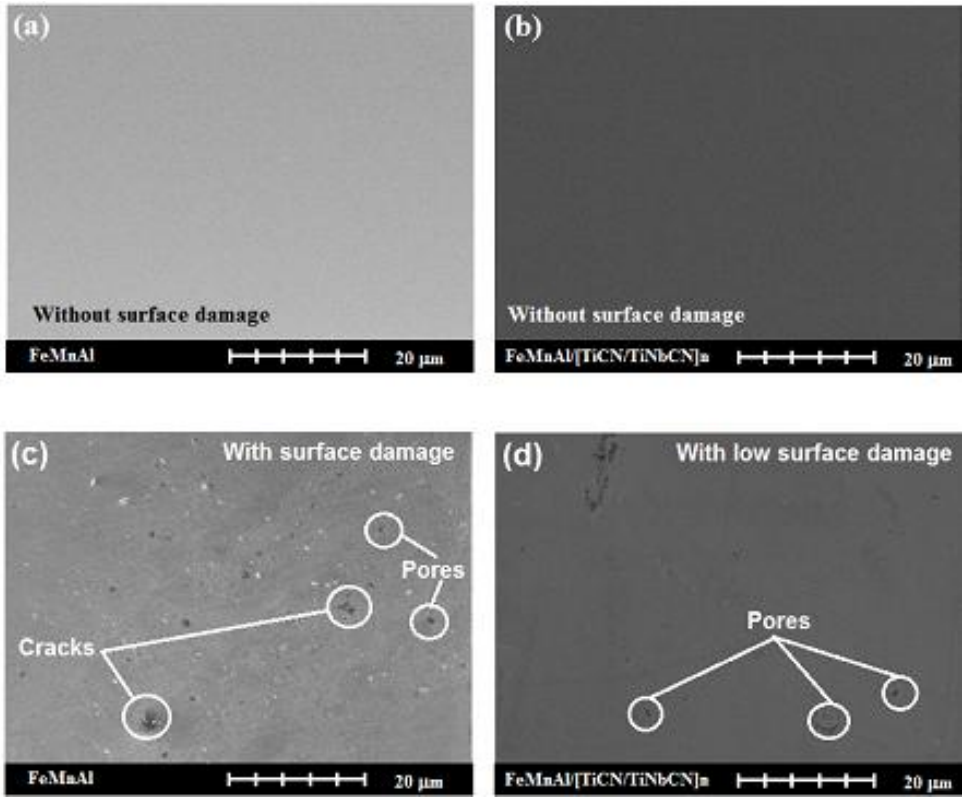

Figure 7. SEM micrographs for samples with and without degradation (a) Fermanal Steel, without exposure: (b) FeMnAl/[TiCN/TiNbCN]n with n = 150 bilayers without exposure; c) Fermanal Steel, with exposure to Hanks solution for a period of 192 hours, and (d) FeMnAl/[TiCN/TiNbCN]n with n = 150 and exposure to Hanks solution for a period of 192 hours.

3.4 Identification of corrosion products

Figure 8 shows the corrosion products of Fermanal steel. The peaks that can be seen are characteristic of the corrosion products that are normally found on the surface of this material, such as

Hematite (Fe_2O_3), manganese oxide (Mn_2O_3) and $Fe_2Al_2O_4$ [29]. These surface compounds are responsible for loss due to dissolution of the passivating layer. This result is in agreement with the surface analysis of corrosion products by SEM (Figure 7). Evidence of corrosion products was not found on the multilayers with n=1, n=50 and n=150.

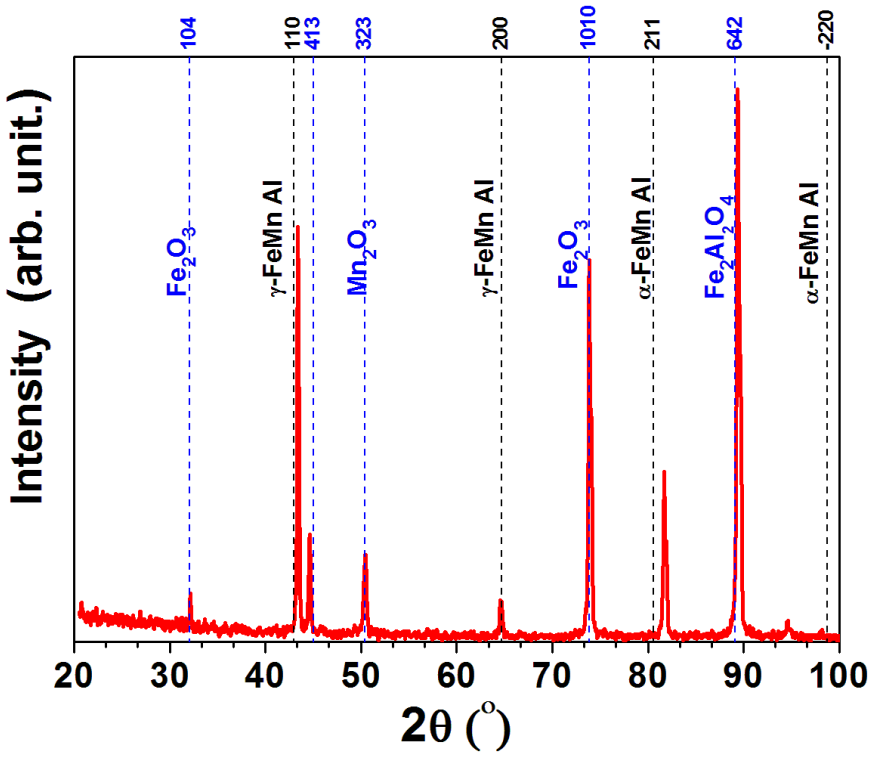

Figure 8. Diffractogram of the Fermanal alloy sample γ = austenite; α= ferrite;ψ = Fe_2O_3; ϖ = Mn_2O_3.

4. CONCLUSIONS

The electrochemical impedance spectroscopy results indicate that the Fermanal steel coated with [TiCN/TiNbCN]n heterostructures shows that the multilayers perform well, as there is apparent increased protection against highly corrosive phenomena. A trend of increased protective effect with the increase in the number of bilayers can also be seen.

In this article it has been shown that the application of up to 150 bilayers improves corrosion resistance of surfaces in contact with Hanks solution. This represents a technique for improving the performance of these multilayers in the hostile environment generated by the human body; as such environments influence the material by changing its characteristics.

The erosion observed by SEM demonstrates the high level of degradation of the FeMnAl alloy, which contrasts the findings observed on the multilayers. Of the corrosion products found on the Fermanal using XRD, it can be said that the manganese oxide improves performance against corrosion, while corrosion products were not found for the coated samples. It can therefore be stated that the results obtained for the Fermanal steels show adequate performance in terms of corrosion resistance in

a physiological medium. In addition, this performance is improved with the application of coatings which lead to enhanced electrochemical properties.

ACKNOWLEDGEMENTS
This research was supported by "El patrimonio Autónomo Fondo Nacional de Financiamiento para la Ciencia, la Tecnología y la Innovación Serveis Científico-Francisco José de Caldas" under contract RC-No. 275-2011, and Universidad Militar Nueva Granada. The authors also wish to acknowledge the technical support of the Universitat de Barcelona.

References

1. R. Langer, L. G. Cima, J. A. Tamada, E. Wintermantel, *Biomaterials* 11 (1990) 738.
2. S.D. Cook, K.A. Tomas, A.F Harding, A. Collings, *Biomaterials* 8 (1986) 177.
3. S. Samuel, S. Nag, T. W. Scharf, R. Banerjee, *Materials Science and Engineering C* 28 (2008) 414.
4. R. Tapash, R. Rautray, K. Kyo-Han, *Progress in Materials Science* 56 (2011) 1137.
5. K. Bordji, J.Y. Jouzeau, D. Mainard, E. Payan, P. Netter, K.T. Rie, T. Stucky, M. Hage-Ali, *Biomaterials* 17 (1996) 929.
6. M. Geetha, A.K. Singh, R. Asokamani, A.K. Gogia, *Progress in Materials Science* 54 (2009) 397.
7. Z. Bou-Saleh, A. Shahryari, S. Omanovic, *Thin Solid Film* 515 (2007) 4727.
8. A. Shahryari, S. Omanovic, J. A. Szpunar, *Materials Science and Engineering: C* 28 (2008) 94.
9. M. Pourbaix, *Biomaterials* 5 (1984) 122.
10. J. Białoń, D. Dudek, K. Kobylańska-Szkaradek, A. Zastawny, *Materials Science and Engineering* 59 (1983) 217.
11. S.C. Tjong, *Materials Characterization* 24 (1990) 275.
12. W. Aperador, A. Vargas, J. Betancur, *Rev. Latin. Am. Metal. Mat.* 32 (2012) 236.
13. V. F. Lins, M. A. Freitas, E. M. Paula e Silva, *Applied Surface Science* 250 (2005) 124.
14. G.A. Pérez Alcázar, *Colomb. Cienc.* 28(107) (2004) 265.
15. C.J. Wang, Y.C. Chang, *Mater. Chem. Phys.* 76 (2005) 151.
16. Y.S. Zhang, X. Lu, X. Tian, Z. Qin, *Materials Science and Engineering* 334 (2002) 19.
17. A.P. Serro, C. Completo, R. Colaço, F. dos Santos, C. Lobato da Silva, J.M.S. Cabral, H. Araújo, E. Pires, B. Saramago, *Surface & Coatings Technology* 203 (2009) 3701.
18. B.H. Moon, H.C. Choe, W. A. Brantley, *Applied Surface Science* 258 (2011) 2088.
19. B. Subramanian, C.V. Muraleedharan, R. Ananthakumar, M. Jayachandran, *Surface & Coatings Technology* 205 (2011) 5014.
20. G. Levi, W. D. Kaplan, M. Bamberger, *Materials Letters* 35 (1998) 344.
21. J. M. Córdoba J. Sayagues, M. D. Alcala and F. J. Gotor, *J. Mater. Chem.* 17 (2007) 650.
22. J. C. Caicedo, C. Amaya, L. Yate, W. Aperador, G. Zambrano, M.E. Gómez, J. Alvarado-Rivera, J. Muñoz-Saldaña, P. Prieto, *Applied Surface Science* 256 (2010) 2876.
23. H. Farnoush, J. Aghazadeh, D. Haghshenas, F. Moztarzadeh, *Ceramics International*, 38 (2012) 4885
24. Željka Petrović, Mirjana Metikoš-Huković, Robert Peter, Mladen Petravić, *Int. J. Electrochem. Sci.*, 7 (2012) 9232 – 9247
25. H. Moreno, J.C. Caicedo, C. Amaya, J. Muñoz-Saldaña, L. Yate, J. Esteve, P. Prieto, *Applied Surface Science* 257 (2010) 1098
26. J.L Polo, E Cano, J.M Bastidas, *Journal of Electroanalytical Chemistry*, 537 (2002) 183.
27. Q. Mohsen, Sahar A. Fadl-allah, and Nahla S. El-Shenawy, *Int. J. Electrochem. Sci.*, 7 (2012) 4510 – 4527

28. N. Diomidis, S. Mischler, N.S. More, Manish Roy, *Acta Biomaterialia*, 8 (2012) 852.
29. M. Bobby Kannan, R.K. Singh Raman, S. Khoddam, *Corrosion Science*, 50 (2008) 2879..

© 2013 by ESG (www.electrochemsci.org)